Available online at www.sciencedirect.com
ScienceDirect
Ceramics International 37 (2011) 3193–3202
CERAMICS INTERNATIONAL
www.elsevier.com/locate/ceramint

Controllable growth of ‘‘multi-level tower’’ ZnO for biodiesel production

Fang Liu, Yong Zhang *

School of Materials Science and Engineering, Dalian Jiaotong University, 794 Huanghe Road, 116028 Dalian, PR China

Received 30 March 2011; received in revised form 16 May 2011; accepted 18 May 2011
Available online 26 May 2011

Abstract

‘‘Multi-level tower’’ ZnO with bulk quantity has been grown by a simple aqueous solution technique. Detailed structural characterization revealed that, the ‘‘multi-level tower’’ ZnO showed perfect hexagonal sectional morphology, with the length and diameter being 1–2 μm and 200–300 nm, respectively. When ‘‘multi-level tower’’ ZnO was used as the solid base catalyst to synthesize biodiesel, a biodiesel yield of 73.5% was achieved, much higher than the 46.2% of particle-like ZnO. Preferred nucleation and growth of ZnO nuclei along [0 0 0 1] direction resulted in hexagonal rod-like ZnO, and further layer-by-layer stacking of rod-like ZnO led to ‘‘multi-level tower’’ architectures, which predominantly exposed active O^{2-} on (0 0 0 2), (1 0 $\bar{1}$ 0), (0 1 $\bar{1}$ 0) and ($\bar{1}$ 1 0 0) planes of ZnO, resulting in obvious enhancement of catalytic activity and high yield of biodiesel.

Keywords: D. ZnO; Hexagonal; Catalyst; Biodiesel

1. Introduction

Dimensionality-, morphology-, and structure-controlled growth of micro/nano materials to achieve distinctive geometries, novel physical and chemical properties has attracted numerous attention. Diverse morphologies of ZnO micro/nano architectures, such as nanorod [1], nanobelt [2], nanoring [3], as well as rod-on-rod [4] and star-shaped [5] nanostructures have been grown, leading to their unique electric, catalytic, optical and photo-chemic properties.

Recently, the catalytic properties of ZnO and zinc hydroxides to synthesize biodiesel, a new kind of renewable and clean energy [6], are drawing new interests [7–10]. Lithium-doped ZnO [7] and zinc hydroxide nitrate [8] have been used as heterogeneous catalysts, in which the biodiesel yields of 96.3% and 93.2% were achieved, respectively. ZnO–La_2O_3 mixed oxide catalyst grown via the co-precipitation approach exhibited a biodiesel yield of 96.0% [9]. Compared with the strong catalytic properties in photo-catalytic and optical fields [1,4], however, the catalytic property of ZnO to synthesize biodiesel is still weak, which is only about 30.0% [10]. Considering the urgent marketable application of biodiesel, growth of effective ZnO catalyst has become a big challenge.

It is newly reported that, the polyhedral evolution of Ru, Pt and Co_3O_4 nanoparticle catalysts, is an important factor to enhance their catalytic properties, because catalytic active planes and active species are predominantly exposed in these cases [11–13]. Because O^{2-} is the strong basic site in catalytically synthesizing biodiesel [9], an interesting idea arises: will shape-controlled growth of polyhedral ZnO-based catalysts and predominant exposure of catalytic active O^{2-}, be effective to improve their catalytic properties?

Herein, we report a simple aqueous solution approach to grow ‘‘multi-level tower’’ ZnO, which showed hexagonal sectional morphology, as well as good catalytic properties for the synthesis of biodiesel. The growth mechanism of ‘‘multi-level tower’’ ZnO was proposed, and the influence of ZnO morphology upon its catalytic properties to synthesize biodiesel was thoroughly discussed. To the best of our knowledge, shape-controlled growth of solid catalysts to synthesize biodiesel has rarely been reported, elsewhere.

2. Experimental procedure

In a typical experiment, certain amount of NaOH was dissolved in 200 mL deionized water, in which the pH value is about 10. Then, 0.01 mol of $ZnCl_2$ was added to this solution, and treated at 60° C for 6 h. The obtained solid products were thoroughly washed and filtered by deionized water, then dried at 60° C.

* Corresponding author. Tel.: +86 0411 84105850; fax: +86 0411 84106828.
E-mail address: zhangyong0411@126.com (Y. Zhang).

0272-8842/$36.00
doi:10.1016/j.ceramint.2011.05.087

The morphology of reaction products was observed using energy dispersive spectrometer (EDS) attached scanning electron microscopy (SEM, JSM-6360LV, with an accelerating voltage of 20 kV, secondary electron image) and high resolution transmission electron microscopy (HRTEM, JEOL2011, with an accelerating voltage of 200 kV). The crystallographic characterization was performed by an X-ray diffraction (XRD, D/Max-Ultima$^+$, with an accelerating voltage of 40 kV) with Cu Kα radiation at a scanning speed of 6°/min.

In reference of previous report [14], the transesterification reactions were carried out in a 100 mL glass reactor with a condenser. Firstly, the solid catalyst was dispersed in methanol under magnetic stirring. Then, soybean oil (AR, Dalian Shenlian Chemical Co., Dalian) was added to the mixture and heated to 60° C. The magnetic stirring rate was 1000 rpm, and the transesterification lasted for 2 h. Samples were taken out from the reaction mixture every 5 min and solid catalyst was separated by centrifugation. Finally, the excess methanol was distilled off under vacuum. After removal of the glycerol layer, the biodiesel was collected, and the yield of biodiesel was calculated according to the equation of previous report [14].

3. Results and discussion

3.1. Characterization of morphology and structure

SEM observation of the as-synthesized product is shown in Fig. 1. Abundant rod-like crystals are found, in which their

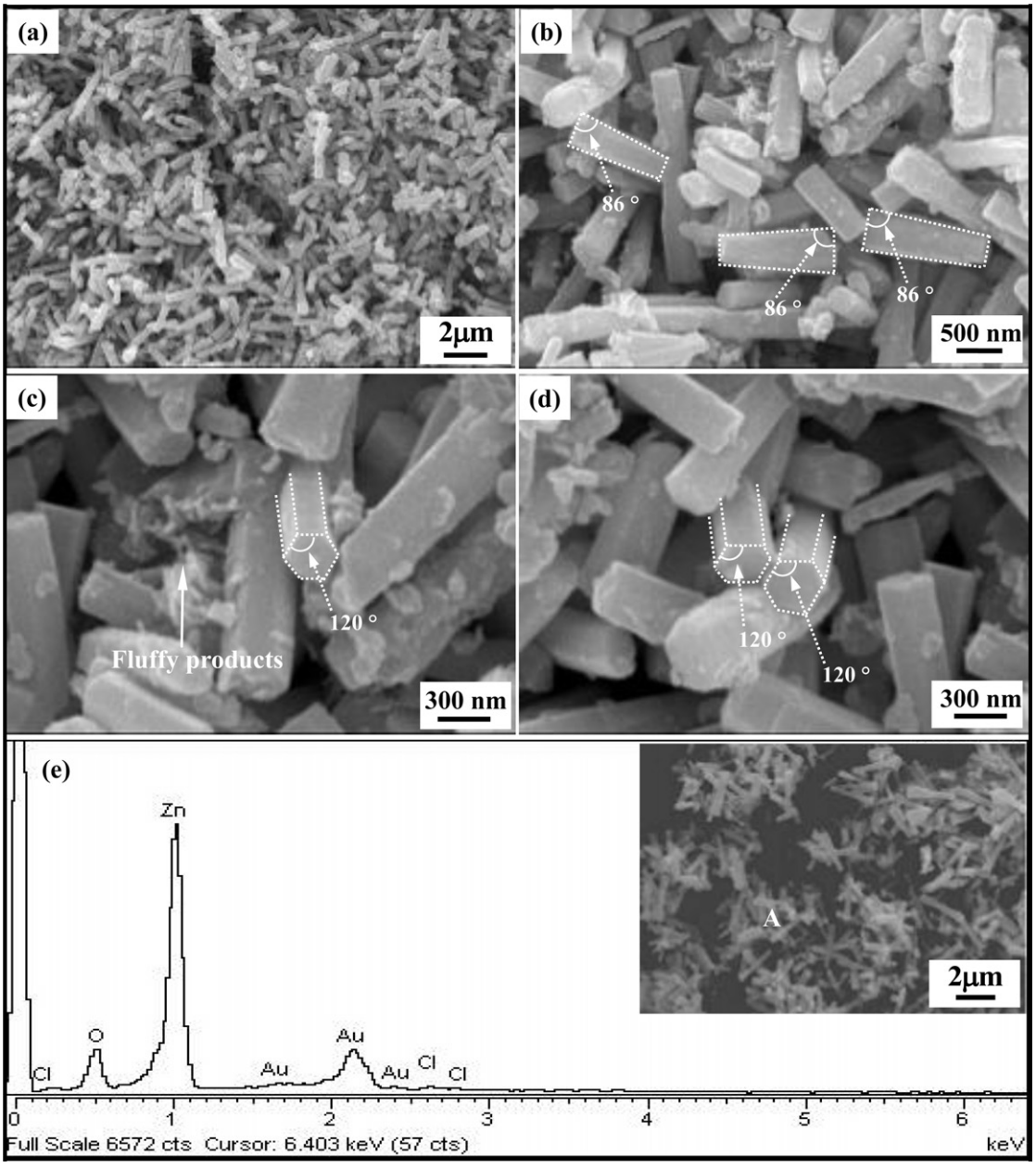

Fig. 1. SEM morphology (a–d) and EDS (e) analysis of the as-prepared sample, where, EDS analysis is performed at point "A" in the inset of (e).

length and diameter are 1–2 μm and 200–300 nm, respectively. These rod-like crystals exhibit the frustum of a prism morphology, with the angle between basal and lateral edges being 86° (Fig. 1(a) and (b)). Additionally, they exhibit the hexagonal sectional morphology, with the internal angle between adjacent well-faced edges being mostly 120° (Fig. 1(c) and (d)), which is close to the internal angle of hexagon.

Fluffy precipitates on big hexagonal rod-like products are shown, as indicated by the white arrow in Fig. 1(c). EDS analysis of the rod-like products and fluffy precipitates (point "A" in the inset of Fig. 1(e)) demonstrates that, Zn and O are their main elements, indicating the formation of ZnO in our experiment. Due to the gold spray treatment before SEM characterization, Au element appears in the EDS spectra.

HRTEM characterization of rod-like ZnO is exhibited in Fig. 2, in which its frustum of a prism morphology is obviously observed. Magnification of a_1 and a_2 areas in Fig. 2(a) further reveals that, steps exist at the middle of one big rod (Fig. 2(a_1) and (a_2)), indicating that the big rod is connected by two small rods. Interestingly, a small rod is grown on one big rod, forming a "two-level tower" at nanometer scale (Fig. 2(a_3)); several steps are found in one big rod, forming a "multi-level tower" architecture (Fig. 2(b)).

In order to understand the growth mechanism of "multi-level tower" ZnO, its morphology evolution as a function of pH value (8, 10 and 12) is examined (Fig. 3). For simplicity, these three samples are called sample-8, sample-10 and sample-12 hereafter. Sample-8 exhibits the polygonal plate morphology, with the internal angle between adjacent edges being mostly 120°. The size and thickness of these plate-like crystals are 1–5μm and 100–200 nm, respectively (Fig. 3(a) and (b)). Fluff and small plate precipitates on big polygonal plates are also found, as indicated by the white arrows in Fig. 3(b).

In the sample-10 case, rod-like crystals are found, which exhibit the frustum of a prism morphology (Fig. 3(c) and (d)). In the case of sample-12, they evolve into small nanoparticles less than 300 nm (Fig. 3(e) and (f)). These results demonstrate that, pH value is the key for controlling the morphology evolution of ZnO micro/nano-architectures.

XRD patterns of sample-8, sample-10 and sample-12 are demonstrated in Fig. 4, which reveal that wurtzite structural ZnO is the main product, with small amount of $Zn(OH)_2$ found. The strong peaks at 31.1° and 34.5° indicate the preferred

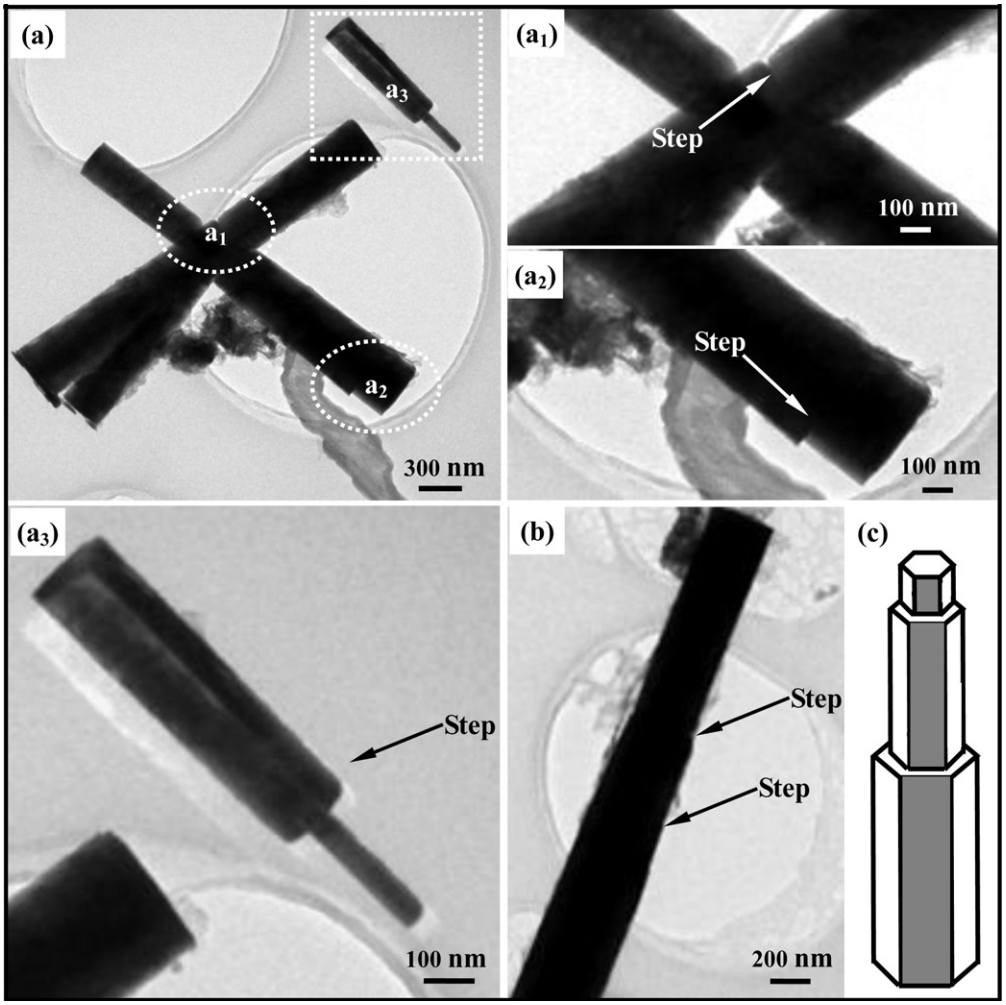

Fig. 2. HRTEM images of the as-prepared sample (a and b) and configuration profile of "multi-level tower" (c), where (a_1), (a_2) and (a_3) are enlargement of areas a_1, a_2, and a_3 in (a), respectively.

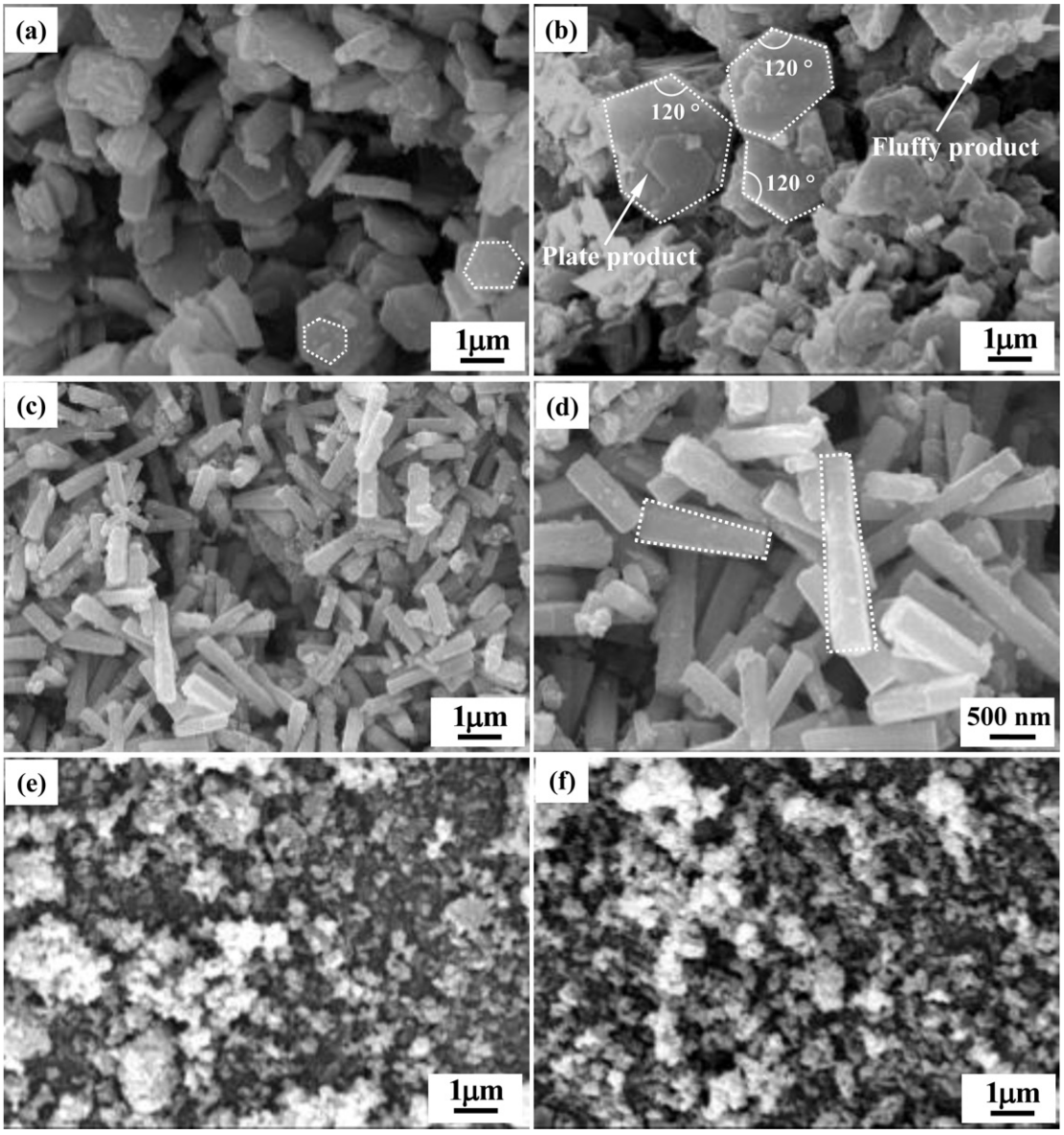

Fig. 3. SEM images of the as-prepared samples at pH value of 8 (a and b), 10 (c and d) and 12 (e and f).

growth of ZnO$(1\,0\,\bar{1}\,0)$ and ZnO(0 0 0 2) planes, respectively (JCPDS card, 65-3411), and the peaks at 24.8°, 28.2°, 30.3°, 33.5° and 37.8° are corresponded to $(1\,1\,\bar{2}\,0)$, $(1\,0\,\bar{1}\,3)$, $(2\,0\,\bar{2}\,1)$, $(2\,0\,\bar{2}\,2)$ and $(2\,0\,\bar{2}\,3)$ planes of ZnO, respectively (JCPDS card, 01-1136). As far as sample-8 is concerned, there is no obviously preferred growth direction of ZnO (Fig. 4(a)). With the increasing of pH value, preferred growth of (0 0 0 2) plane is found in sample-10 (Fig. 4(b)). When the pH value is 12, sample-12 exhibits disordered growth again (Fig. 4(c)).

HRTEM characterization further reflects the facet selective growth character of sample-10. As shown in Fig. 5(a), (c) and (e), plate-like, ''multi-level tower'' and particle-like crystals are exhibited in sample-8, sample-10 and sample-12, respectively. The interplanar spacing of plate-like crystal is about 0.28 nm (Fig. 5(b)), corresponding to the distance between two $(1\,0\,\bar{1}\,0)$ planes of ZnO. The ''multi-level tower'' crystal exhibits an interplanar spacing of about 0.26 nm (Fig. 5(d)), indicating the preferred growth of ZnO(0 0 0 2) plane, in agreement with the above XRD analysis. Additionally, the interplanar spacings of 0.16 nm and 0.15 nm of small nanoparticles are corresponded to $(1\,1\,\bar{2}\,0)$ and $(1\,0\,\bar{1}\,3)$ planes of ZnO, respectively (Fig. 5(f)).

3.2. Growth mechanism of "multi-level tower" ZnO

The facet selective growth of micro/nano-architectures is determined by the energeticably favorable growth principle, which may be helpful to understand the growth mechanism of ''multi-level tower'' ZnO. In basic solutions, the predominantly existed zinc soluble species is $[Zn(OH)_4]^{2-}$, which is considered to be the growth unit of ZnO [15], because $[Zn(OH)_4]^{2-}$ transforms to ZnO according to the following reactions [15,16]:

$$[Zn(OH)_4]^{2-} \rightarrow Zn(OH)_2(s) + 2OH^- \quad (1)$$

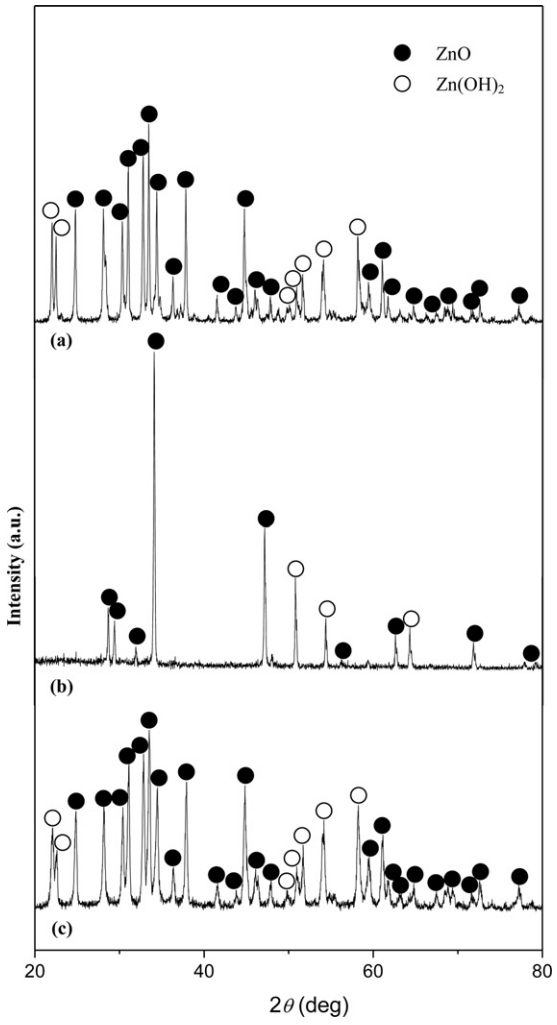

Fig. 4. XRD patterns of sample-8 (a), sample-10 (b) and sample-12 (c).

$$Zn(OH)_2(s) \rightarrow ZnO(s) + H_2O \quad (2)$$

As a result, the adsorption of $[Zn(OH)_4]^{2-}$ on different energetically favorable growth planes determines the morphology evolution. Generally, [0 0 0 1] is the most energetically favorable growth direction of wurtzite structural ZnO, because of its alternative stacking structure of O^{2-} and Zn^{2-} along *c*-axis [17,18]; the addition of structure-directing agents (for example, ethylenediamine, NaCl and KCl) in basic solution also leads to the second energetically favorable growth of $(1\,0\,\bar{1}\,0)$, $(1\,1\,\bar{2}\,0)$, $(2\,\bar{1}\,\bar{1}\,0)$ and other planes [15,19].

In our basic environment, the formation of $Zn(OH)_2$ (Fig. 4) indicates the transformation from $[Zn(OH)_4]^{2-}$ to ZnO; the preferred growth of (0 0 0 2) plane (Fig. 4) indicates its preferred growth along [0 0 0 1] direction [20]. Thus, adsorption of $[Zn(OH)_4]^{2-}$ on (0 0 0 2) plane and growth along [0 0 0 1] direction is the most energetically favorable, resulting in rod-like ZnO. Because of the introduction of Cl^- from $ZnCl_2$, the second energetically favorable growth of $(1\,0\,\bar{1}\,0)$ plane appears [15], which indicates the lateral preferred growth of $\{1\,0\,\bar{1}\,0\}$ planes of rod-like ZnO [20]. Consequently, rod-like ZnO bounded by (0 0 0 2), $(1\,0\,\bar{1}\,0)$, $(0\,1\,\bar{1}\,0)$, $(\bar{1}\,1\,0\,0)$, $(\bar{1}\,0\,1\,0)$, $(1\,\bar{1}\,0\,0)$ and $(0\,\bar{1}\,1\,0)$ planes is achieved, which exhibits hexagonal sectional morphology (Fig. 1), because of the 120° internal angle between $\{1\,0\,\bar{1}\,0\}$ planes.

Due to the good lattice matching, (0 0 0 2) plane of hexagonal rod-like ZnO is a good nucleation site for the ZnO nuclei to nucleate, which results in big hexagonal plate on rod-like ZnO. With the continuous emergence of $[Zn(OH)_4]^{2-}$, plate-like ZnO also grow into rod-like morphology on the first rod-like one, because of its mainly preferred growth of (0 0 0 2) plane and lateral preferred growth of $\{1\,0\,\bar{1}\,0\}$ planes, forming "two-level tower" ZnO (Fig. 2(a_1) and (a_2)). Similarly, newly arriving ZnO nuclei will further nucleate and grow on the (0 0 0 2) plane of "two-level tower" ZnO, forming "multi-level tower" architecture (Fig. 2(b)). This layer-by-layer stacking mechanism is shown in Fig. 6.

Shape-controlled growth of ZnO micro/nano-structures is an interesting topic all the time, because of its unique physical and chemical properties. Many experimental factors, such as basicity, structure-directing agents, reaction temperature and substrate play important roles for the morphology evolution of ZnO, in which NaOH is the most versatile factor to adjust basicity and achieve wurtzite ZnO [21]. Aligned ZnO nanorod has been grown in basic solution [22]. Wang et al. [23] found that, with the increasing of pH value in solution, strip-shaped ZnO evolved into short column-shaped product.

According to reactions (1) and (2) in our experiment, the amount of NaOH is crucial for the transformation from $[Zn(OH)_4]^{2-}$ to ZnO, thus determining the morphology evolution of ZnO. When the pH value is 10, suitable amount of $[Zn(OH)_4]^{2-}$ is provided in sample-10, which is adsorbed on (0 0 0 2) plane for the nucleation and growth of ZnO. In this case, layer-by-layer stacking of rod-like ZnO leads to "multi-level tower" architectures.

In the case of sample-8, the pH value is 8, however, there is not enough $[Zn(OH)_4]^{2-}$ for the nucleation and growth of ZnO, just resulting in plate-like ZnO with 100–200 nm thickness. When the pH value is increased to 12, too much $[Zn(OH)_4]^{2-}$ exists in sample-12, which covers (0 0 0 2), $(1\,0\,\bar{1}\,0)$, $(1\,1\,\bar{2}\,0)$ and all the other planes for the nucleation and growth of ZnO. As a result, ZnO loses its preferred growth of (0 0 0 2) and $\{1\,0\,\bar{1}\,0\}$ planes, leading to disordered growth and the formation of small nanoparticles.

Structure-directing agent is another important factor to determine the final morphology of ZnO. Usually, low index crystal planes of nanostructures such as {1 0 0}, {1 1 1} and {1 1 0} planes are more thermodynamically stable than other facets, to fulfill the smallest surface energy principle [24]. When organic or inorganic agents are added, however, the surface energies of these facets are changed, leading to newly unique morphologies of micro/nano-structures. With the addition of ethylenediamine, ZnO pyramid-like hierarchical micro/nano-architectures have been grown [19]. Rod-like ZnO has also been found, when Cl^- is introduced, and our experiment result is similar with this report [15].

Reaction temperature and substrate also play vital roles for the morphology evolution of ZnO. With the increasing of

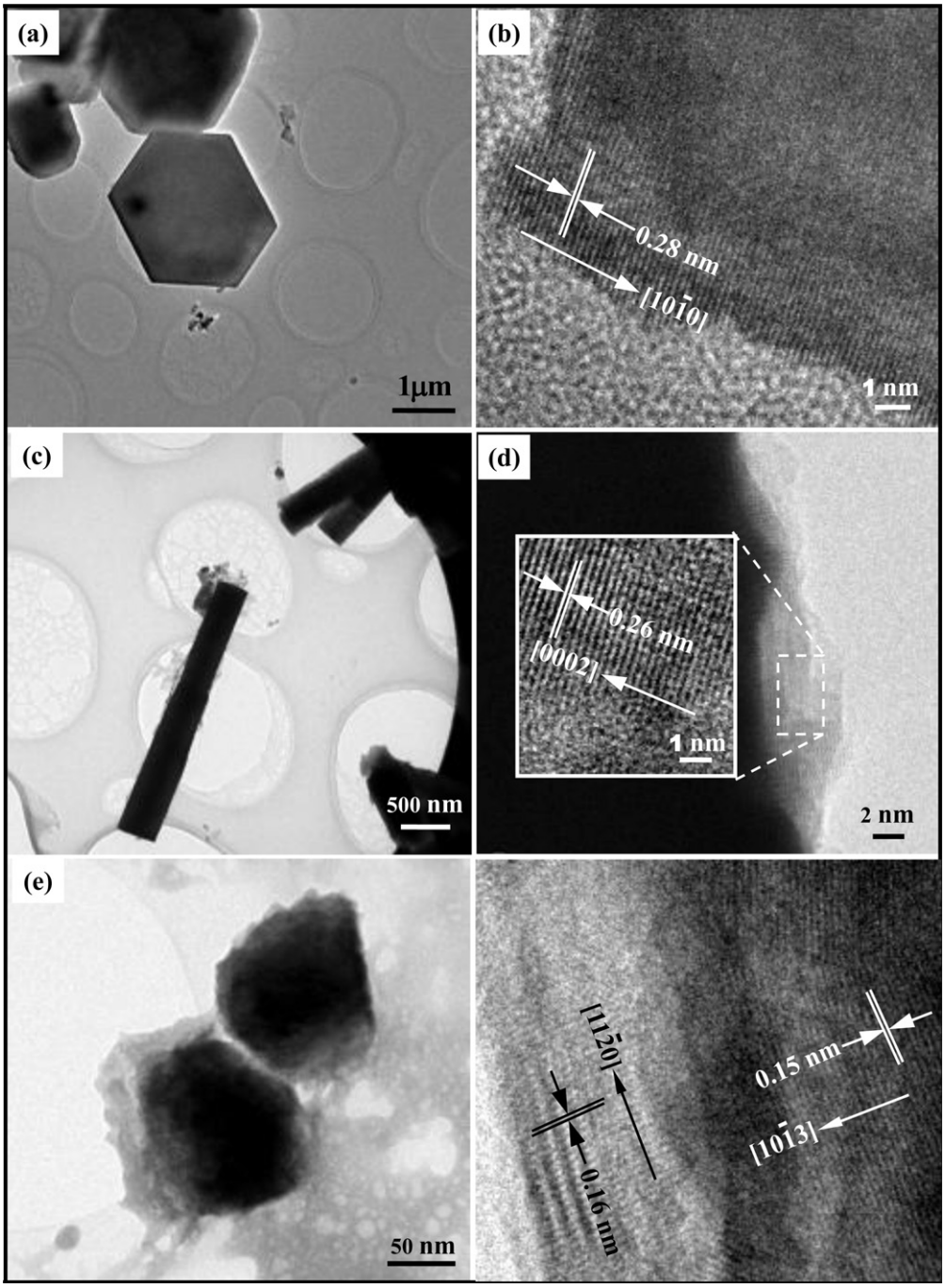

Fig. 5. HRTEM images of sample-8 (a and b), sample-10 (c and d) and sample-12 (e and f).

reaction temperature, morphology evolution of ZnO from long strip to short column has been reported [23]. Generally, the solution phase growth of various morphological ZnO is above 70 °C [5,16,17]. Because of the low reaction temperature (60° C) in our basic experiment, transformation from $Zn(OH)_2$ to ZnO may not proceed completely, which results in the formation of small amount of $Zn(OH)_2$, precipitating as fluffy products on the surface of ''multi-level tower'' and plate-like ZnO (Figs. 1(c) and 3(b)). As far as reaction substrate is concerned, different crystal planes exhibit different facet-selective inducing abilities for the nucleation and growth of ZnO nanorods [22]. Because no substrate is used in our experiment, its influence upon the morphology evolution of ZnO is not found.

Based on the above analysis, layer-by-layer nucleation and growth of hexagonal rod-like ZnO leads to ''multi-level tower'' ZnO, in which pH value of solution phase is the key for controlling the morphology evolution. This is different from the growth mechanism of rod-on-rod ZnO reported by Fan et al. [4], which is performed under the thermal evaporation environment, with growth temperature playing a key role for the morphology evolution.

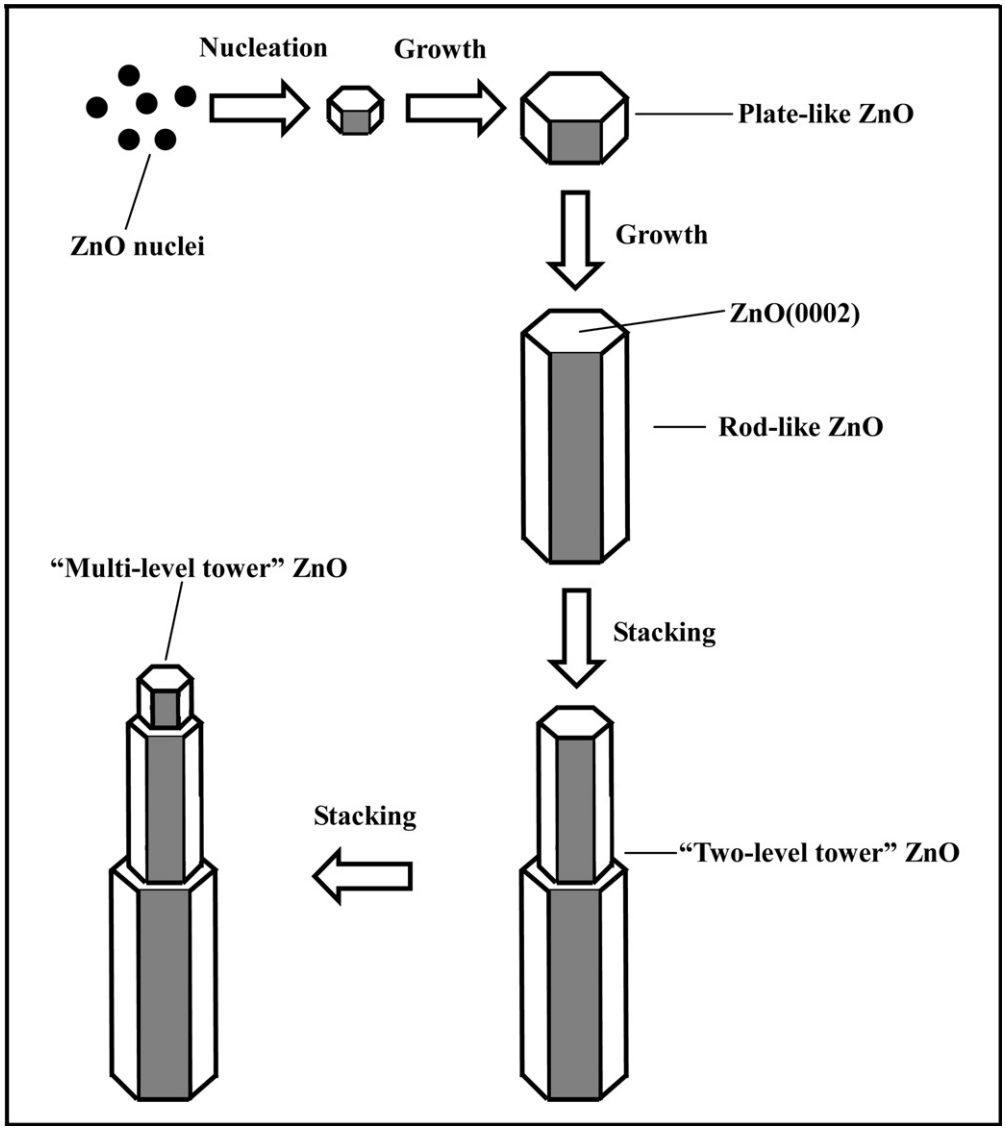

Fig. 6. Schematic illustration for the formation of ''multi-level tower'' ZnO.

3.3. Catalytic properties of "multi-level tower" ZnO in trans-esterification reaction

Different morphologies of ZnO are used as solid base catalysts, and the effect of morphology on the biodiesel yield is shown in Fig. 7. The yield of biodiesel firstly increased and then decreased, when the morphology of ZnO evolves from plate-like to ''multi-level tower'' and particle-like. ''Multi-level tower'' is the optimum morphology in our experiment, in which a biodiesel yield of 73.5% is achieved.

Biodiesel is attracting more and more attention, because of its renewable, biodegradable and nontoxic advantages as a new kind of clean energy for transportation sector [6]. Conventionally, biodiesel is produced through the transesterification of triglycerides from vegetable oils and animal fats with monoalkyl alcohols, such as methanol. Due to the advantages such as noncorrosion, environmental benignancy and easy separation from liquid products, heterogeneous solid base catalysts are

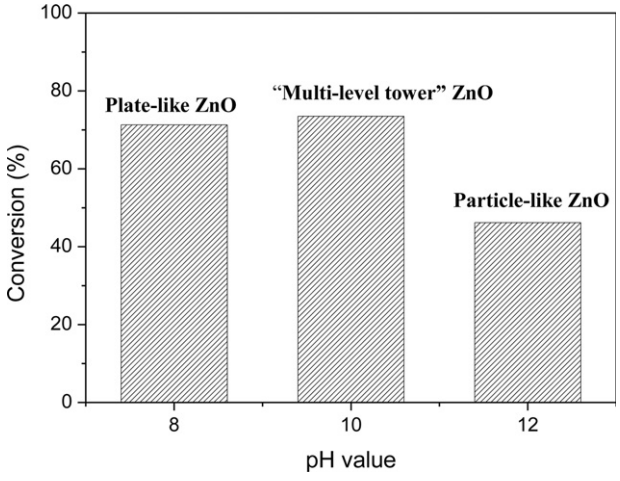

Fig. 7. Effect of ZnO morphology on the yield of biodiesel.

being widely used for the transesterification of triglycerides. Though a number of solid base catalysts have been reported to produce biodiesel [8–10,14,25,26], their marketable applications remain elusive.

Morphology control of catalysts is effective to enhance their catalytic activities. Because catalysis reaction is sensitive to certain surface structures or facets of catalyst particles, the catalytic activity can be enhanced on some favorable facets. Typically, it is possible to expose some favorable facets by controlling the morphology of catalyst particles [13]. It has been shown that, O^{2-} is the predominantly strong basic site of layer structured Mg–Al hydrotalcites and MgO [27], as solid base catalysts to synthesize biodiesel. The lattice oxygens on the surface of ZnO are also considered as basic sites for the transesterification reactions. With the increase of surface lattice oxygens by La doping, enhanced catalytic properties of ZnO have been reported, with a biodiesel yield of 96.0% achieved [9]. Thus, predominant exposure of O^{2-} on favorable facets is promising to enhance the catalytic properties of ZnO solid base catalysts.

ZnO has a wurtzite structure, in which O^{2-} and Zn^{2-} related planes are alternatively stacked along *c*-axis [18]. Actually, it is cross linked by O^{2-} hexagonal close-packed (hcp) structure and Zn^{2-} hcp structure, respectively. Because the diameter of O^{2-} (0.26 nm) is much larger than that of Zn^{2-} (0.15 nm) [28], the framework of wurtzite structure is regarded as O^{2-} hcp, with the tetrahedral interstice occupied by Zn^{2-} hcp, as shown in Fig. 8(a). As a result, O^{2-} is predominantly exposed on (0 0 0 2) basal plane (Fig. 8(b)), favorable to achieve high catalytic activity. When plate-like ZnO is used to synthesize biodiesel, high biodiesel yield of 71.3% is achieved. In addition to (0 0 0 2) basal plane, active O^{2-} is also predominantly exposed on $(1\,0\,\bar{1}\,0)$, $(0\,1\,\bar{1}\,0)$ and $(\bar{1}\,1\,0\,0)$ lateral planes of "multi-level tower" ZnO (Fig. 8(c)–(e)), with 73.5% of

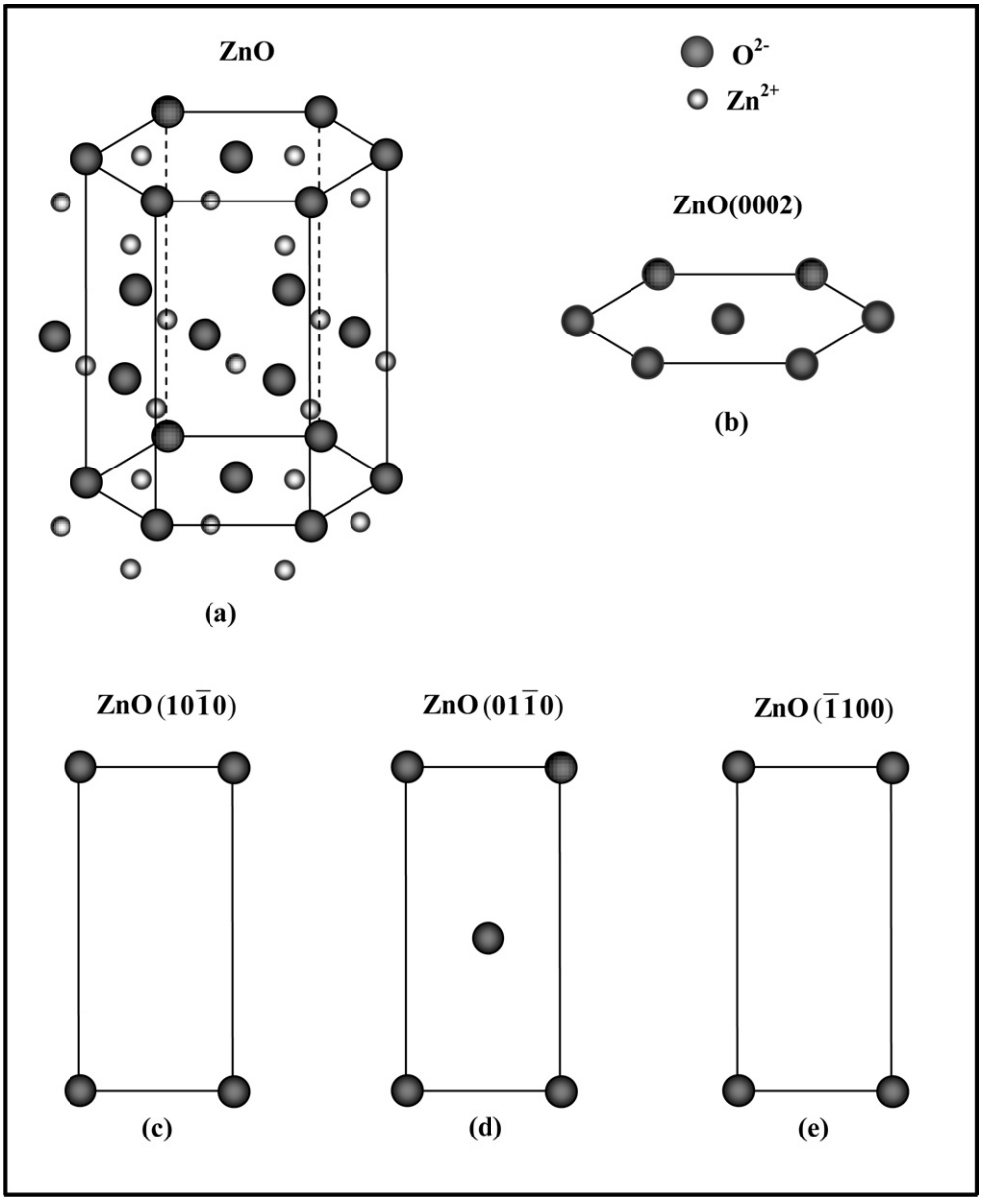

Fig. 8. (a) Structure model of ZnO; (b–e) surface atomic configurations on the (0 0 0 2), $(1\,0\,\bar{1}\,0)$, $(0\,1\,\bar{1}\,0)$ and $(\bar{1}\,1\,0\,0)$ planes of ZnO, respectively.

biodiesel yield achieved. In the case of particle-like ZnO, there is no favorable plane to predominantly expose active O^{2-}, in which the biodiesel yield is only 46.2%.

Though weak catalytic activity is always observed for ZnO to synthesize biodiesel [10], shape-controlled growth of ''multi-level tower'' ZnO predominantly expose active O^{2-} on (0 0 0 2) and other planes, leading to obvious enhancement of catalytic activity and high yield of biodiesel. Because the rough surface containing terraced, stepped and kinked sites is more active than a flat, low index surface [13,29], the steps appeared in ''multi-level tower'' ZnO may also contribute to the enhancement of biodiesel yield. Considering the catalytic activity of OH^- to synthesize biodiesel [8], formation of $Zn(OH)_2$ in this paper is also favorable to enhance the yield of biodiesel.

In order to verify this hypothesis, FT-IR spectroscopy characterization of plate-like, ''multi-level tower'' and particle-like ZnO of sample-8, sample-10 and sample-12, respectively, is performed, which is shown in Fig. 1S. Obviously, there are strong bands corresponding to hydroxyl groups (O–H) between 2900 and 3500 cm^{-1} [30], and the bands near 1400–1600 cm^{-1} and 700–900 cm^{-1} are identified as carboxylate stretches, arising from the adsorption of atmospheric H_2O and CO_2 on the surface of ZnO [30,31], respectively. The bands between 450 and 650 cm^{-1} are assigned to the stretching vibrations of Zn–O [30]. Compared with particle-like ZnO, the bands of plate-like and ''multi-level tower'' ZnO demonstrate ''red-shift'' trend, which may be resulted from their much larger size than particle-like ZnO (Fig. 3). Different from the Zn–O bond of particle-like ZnO centered at 466 cm^{-1}, plate-like and ''multi-level tower'' ZnO exhibit much stronger bands at 468 cm^{-1}, together with the appearance of new bands centered at 569 cm^{-1}, confirming the high catalytic activity of plate-like and ''multi-level tower'' ZnO in synthesizing biodiesel proposed above.

Moreover, the weak bands near 1010–1040 cm^{-1} are attributed to the OH group bending in Zn–OH entities [32], confirming the existence of fluffy $Zn(OH)_2$ in our experiment. In order to completely convert fluffy $Zn(OH)_2$ into ZnO, the above ''multi-level tower'' ZnO sample is calcined under 500° C for 2 h. Weighing the mass changes before and after calcination, the weight percentage of $Zn(OH)_2$ and ''multi-level tower'' ZnO in this sample is calculated to be 5.2% and 94.8%, respectively, according to reaction (2). As solid base catalyst, a biodiesel yield of 75.1% is achieved from the calcined sample, which can be considered as the catalytic contribution of ''multi-level tower'' ZnO with no $Zn(OH)_2$ participated, different from the 73.5% yield of sample-10 in Fig. 7, which resulted from the compounded contribution of ''multi-level tower'' ZnO and fluffy $Zn(OH)_2$.

Assuming that the catalytic properties of ''multi-level tower'' ZnO, fluffy $Zn(OH)_2$ and their compounded contribution in synthesizing biodiesel are *Y*1, *Y*2 and *Y*, respectively, the following equation can be obtained

$$Y1 \times 94.8\% + Y2 \times 5.2\% = Y \quad (3)$$

Because the values of *Y*1 and *Y* are 75.1% and 73.5%, respectively, *Y*2 can be calculated as 44.3%. Hence, the high catalytic activity in synthesizing biodiesel, is mainly from ''multi-level tower'' ZnO, not fluffy $Zn(OH)_2$.

Compared with ZnO and $Zn(OH)_2$, CaO [33], MgO [34], SrO [14] and their hydroxides exhibit much higher catalytic activity than ZnO to synthesize biodiesel, shape-controlled growth of these solid base catalysts to predominantly expose active O^{2-} or OH^- on favorable planes, may further increase their catalytic activity and accelerate the marketable application of biodiesel. The experimental results in this paper may also be helpful for the shape-controlled growth of newly distinctive morphologies of ZnO, as well as exploring their novel catalytic properties.

4. Conclusions

''Multi-level tower'' ZnO architectures with hexagonal sectional morphology, were grown by a simple aqueous solution approach. Their length and diameter were 1–2μm and 200–300 nm, respectively. When ''multi-level tower'' ZnO was used as the solid base catalyst to synthesize biodiesel, a biodiesel yield of 73.5% was achieved, much higher than the 46.2% of particle-like ZnO. Layer-by-layer nucleation and growth of hexagonal rod-like ZnO led to ''multi-level tower'' ZnO, which predominantly exposed active O^{2-} on (0 0 0 2), $(1\,0\,\bar{1}\,0)$, $(0\,1\,\bar{1}\,0)$ and $(\bar{1}\,1\,0\,0)$ planes, resulting in obvious enhancement of catalytic activity.

The shape-controlled growth of ''multi-level tower'' ZnO architectures in this paper, may give some good suggestions to increase the yield of biodiesel, accelerating its marketable application. Moreover, it may also be helpful to grow new distinctive morphologies of ZnO, as well as exploring their novel catalytic properties.

Appendix A. Supplementary data

Supplementary data associated with this article can be found, in the online version, at doi:10.1016/j.ceramint.2011.05.087.

References

[1] Y.X. Wang, X.Y. Li, G. Lu, G.H. Chen, Y.Y. Chen, Synthesis and photocatalytic degradation property of nanostructured-ZnO with different morphology, Mater. Lett. 62 (2008) 2359–2362.
[2] Z.W. Pan, Z.R. Dai, Z.L. Wang, Nanobelts of semiconducting oxides, Science 291 (2001) 1947–1949.
[3] X.Y. Kong, Y. Ding, R.S. Yang, Z.L. Wang, Single-crystal nanorings formed by epitaxial self-coiling of polar nanobelts, Science 303 (2004) 1348–1351.
[4] D.H. Fan, R. Zhang, X.H. Wang, Synthesis and ultraviolet emission of aligned ZnO rod-on-rod nanostructures, Solid State Commun. 150 (2010) 824–827.
[5] H.M. Hu, C.H. Deng, X.H. Huang, Hydrothermal growth of center-hollow multigonal star-shaped ZnO architectures assembled by hexagonal conic nanotubes, Mater. Chem. Phys. 121 (2010) 364–369.
[6] J.M. Marchetti, V.U. Miguel, A.F. Errazu, Possible methods for biodiesel production, Renew. Sust. Energy Rev. 11 (2007) 1300–1311.
[7] W.L. Xie, Z.Q. Yang, H. Chun, Catalytic properties of lithium-doped ZnO used for biodiesel preparations, Ind. Eng. Chem. Res. 46 (2007) 7942–7949.

[8] C.S. Cordeiro, G.G.C. Arizaga, L.P. Ramos, F. Wypych, A new zinc nitrate heterogeneous catalyst for the esterification of free fatty acids and trans-esterification of vegetable oils, Catal. Commun. 9 (2008) 2140–2143.
[9] S.L. Yan, S.O. Salley, K.Y. Simon Ng, Simultaneous transesterification and esterification of unrefined or waste oils over ZnO–La_2O_3 catalysts, Appl. Catal. A: Gen. 353 (2009) 203–212.
[10] W.M. Antunes, C.O. Veloso, C.A. Henriques, Transesterification of soybean oil with methanol catalyzed by basic solids, Catal. Today 133–135 (2008) 548–554.
[11] P. Nolte, A. Stierle, N.Y. Jin-Phillipp, N. Kasper, T.U. Schulli, H. Dosch, Shape changes of supported Rh nanoparticles during oxidation and reduction cycles, Science 321 (2008) 1654–1658.
[12] X.W. Xie, Y. Li, Z.Q. Liu, M. Haruta, W.J. Shen, Low-temperature oxidation of CO catalysed by Co_3O_4 nanorods, Nature 458 (2009) 746–749.
[13] J.Y. Chen, B. Lim, E.P. Lee, Y.N. Xia, Shape-controlled synthesis of platinum nanocrystals for catalytic and electrocatalytic applications, Nano Today 4 (2009) 81–95.
[14] X.J. Liu, H.Y. He, Y.J. Wang, S.L. Zhu, Transesterification of soybean oil to biodiesel using SrO as a solid base catalyst, Catal. Commun. 8 (2007) 1107–1111.
[15] F. Xu, Y.N. Lu, Y. Xie, Y.F. Liu, Controllable morphology evolution of electrodeposited ZnO nano/micro-scale structures in aqueous solution, Mater. Des. 30 (2009) 1704–1711.
[16] S.F. Wang, T.Y. Tseng, Y.R. Wang, C.Y. Wang, H.C. Lu, Effect of ZnO seed layers on the solution chemical growth of ZnO nanorod arrays, Ceram. Int. 35 (2009) 1255–1260.
[17] X.F. Zhou, X.F. Guo, W.P. Ding, Y. Chen, Superhydrophobic or superhydrophilic surfaces regulated by micro-nano structured ZnO powders, Appl. Surf. Sci. 255 (2008) 3371–3374.
[18] X.Y. Kong, Z.L. Wang, Spontaneous polarization-induced nanohelixes, nanosprings and nanorings of piezoelectric nanobelts, Nano Lett. 3 (2003) 1625–1631.
[19] F. Lu, W.P. Cai, Y.G. Zhang, ZnO hierarchical micro/nanoarchitectures: solvothermal synthesis and structurally enhanced photocatalytic performance, Adv. Funct. Mater. 18 (2008) 1047–1056.
[20] C.X. Xu, X.W. Sun, Z.L. Dong, M.B. Yu, Zinc oxide nanodisk, Appl. Phys. Lett. 85 (2004) 3878–3881.
[21] S. Yamabi, H. Imai, Growth conditions for wurtzite zinc oxide films in aqueous solutions, J. Mater. Chem. 12 (2002) 3773–3778.
[22] J.P. Cheng, X.B. Zhang, Z.Q. Luo, Aligned ZnO nanorod arrays fabricated on Si substrate by solution deposition, Physica E 31 (2006) 235–239.
[23] B.G. Wang, E.W. Shi, W.Z. Zhong, Understanding and controlling the morphology of ZnO crystallites under hydrothermal conditions, Cryst. Res. Technol. 32 (1997) 659–667.
[24] H.L. Cao, X.F. Qian, C. Wang, X.D. Ma, J. Yin, Z.K. Zhu, High symmetric 18-facet polyhedron nanocrystals of Cu_7S_4 with a hollow nanocage, J. Am. Chem. Soc. 127 (2005) 16024–16025.
[25] G. Sunita, B.M. Devassy, A. Vinu, D.P. Sawant, V.V. Balasubramanian, S.B. Halligudi, Synthesis of biodiesel over zirconia-supported isopoly and heteropoly tungstate catalysts, Catal. Commun. 9 (2008) 696–702.
[26] O.S. Stamenkovic, M.L. Lazic, Z.B. Todorovic, V.B. Veljkovic, D.U. Skala, The effect of agitation intensity on alkali-catalyzed methanolysis of sunflower oil, Bioresour. Technol. 98 (2007) 2688–2699.
[27] J.J. Di Cosimo, V.K. Diez, M. Xu, E. Iglesia, C.R. Apesteguia, Structure and surface and catalytic properties of Mg–Al basic oxides, J. Catal. 178 (1998) 499–510.
[28] R.C. Weast, Handbook of Chemistry and Physics, 69th ed., CRC Press, USA, 1988.
[29] G.C. Bond, Small particles of the platinum metals, Platinum Met. Rev. 19 (1975) 126–134.
[30] C. Liewhiran, S. Seraphin, S. Phanichphant, Synthesis of nano-sized ZnO powders by thermal decomposition of zinc acetate using *Broussonetia papyrifera* (L.) Vent pulp as a dispersant, Curr. Appl. Phys. 6 (2006) 499–502.
[31] A. Brito, M.E. Borges, M. Garin, A. Hernandez, Biodiesel production from waste oil using Mg–Al layered double hydroxide catalysts, Energy Fuels 23 (2009) 2952–2958.
[32] A. Zieba, A. Pacuła, E.M. Serwicka, A. Drelinkiewicz, Transesterification of triglycerides with methanol over thermally treated $Zn_5(OH)_8(NO_3)_2\times 2H_2O$ salt, Fuel 89 (2010) 1961–1972.
[33] X.J. Liu, H.Y. He, Y.J. Wang, S.L. Zhu, X.L. Piao, Transesterification of soybean oil to biodiesel using CaO as a solid base catalyst, Fuel 87 (2008) 216–221.
[34] E.S. Umdu, M. Tuncer, E. Seker, Transesterification of *Nannochloropsis oculata* microalga's lipid to biodiesel on Al_2O_3 supported CaO and MgO catalysts, Bioresour. Technol. 100 (2009) 2828–2831.